PAPER

Check for updates

Acoustic shock wave-induced superheating-assisted dynamic recrystallization – a case study of D-tartaric acid†

Sivakumar Aswathappa,[a] Lidong Dai, ID *[a] Sahaya Jude Dhas Sathiyadhas[b] and Raju Suresh Kumar ID [c]

Superheating-assisted melting and crystallization are prominent subjects in condensed matter physics. However, understanding the superheating concepts under acoustic shocked conditions remains a mystery. Herein, we demonstrate superheating on the basis of dynamic recrystallization in a D-tartaric acid powder sample, which nearly attains an ideal crystal structure and morphology under the 100-shocked conditions compared to the control sample and the obtained results are evaluated by conventional diffraction, spectroscopic and microscopic techniques. From the XRD results, the intensities of the planes (100) and (110) are found to have increased under the 100-shocked conditions, whereas the intensity ratio (011)/(110) has been significantly reduced. Moreover, the intensity ratio of major internal Raman modes such as v_{C-O} (1694 and 1700 cm^{-1}), v_{C-H} (2933 and 2967 cm^{-1}) and v_{O-H} (3331 and 3403 cm^{-1}) has been considerably modified with respect to the number of shock pulses such that the sample produces an ideal Raman spectrum of D-tartaric acid, and thereby the intensities of the lattice Raman modes also support this claim. Most importantly, the SEM results demonstrate the formation of an ideal morphology of D-tartaric acid from the irregular morphological pattern upon exposure to 100 shocks due to the superheating and dynamic recrystallization process. The proposed technique is strongly suggested for materials processing to enhance technological significance for all classes and scales of materials.

Introduction

Melting-related theories (*e.g.*, the kinetic theory of solids) and studies always have a special benchmark in the physics and chemistry of materials research, which can help clearly understand Earth's and planetary materials' stabilities and their structural dynamics.[1,2] Acquiring knowledge of pressure-dependent melting temperatures of such materials is fundamental, providing a deep insight into the thermal structure and geochemical cycles of the Earth and other planets. Melting can take place in materials under two different thermo-dynamical conditions such as steady-state (static compression)[3] and unsteady-state conditions (dynamic compression).[4] The melting characteristics vary

significantly for the two conditions (for example, heating of ice cubes under thermal equilibrium and non-equilibrium conditions).[5] Generally, the process of heating under unsteady-state conditions is referred to as superheating and crystallization, which is dynamic recrystallization. Superheating is a phenomenon of solids in which they can stay in a solid-state while being overheated above their equilibrium melting point. It often occurs while the heating rate is very high wherein the atoms of solids do not have sufficient time to reach a thermodynamic equilibrium state, which can take place under pulsed laser shockwave irradiation,[6] dynamic flyer-plate shock wave compression[7] and acoustic shocked conditions.[8] Substantial knowledge can be gained from dynamic shock waves to advance the science of dynamic recrystallization and superheating of solid-state materials. Over the years, considerable progress has been made on this fascinating subject with many publications on some aspects of shock wave-induced melting.[6-8] Nonetheless, there is still just a scant amount of knowledge regarding superheating and associated phenomenological concepts on materials under acoustic shocked conditions. According to the literature reports, the impact of acoustic shock waves on materials is not well understood compared to the outcome of laser and flyer plate shock waves on solids.[9,10] Moreover, the heating time scales of flyer plate shock compression and laser

[a] Key Laboratory of High-temperature and High-Pressure Study of the Earth's Interior, Institute of Geochemistry, Chinese Academy of Sciences, Guiyang, Guizhou 550081, China. E-mail: dailidong@vip.gyig.ac.cn

[b] Saveetha School of Engineering, Saveetha Institute of Medical and Technical Sciences, Saveetha University, Chennai, Tamil Nadu, 602105, India

[c] Department of Chemistry, College of Science, King Saud University, P.O. Box 2455, Riyadh 11451, Saudi Arabia

shock waves are of the order of nanoseconds, whereas the heating time of acoustic shock waves falls under milli-to-microseconds.[8] It has been authenticated that the slower rate of dynamic superheating effects facilitates significant changes in the atomic crystal structure and surface morphology because of the dynamic recrystallization process compared to the static and nanosecond shock compression.[11–15] A few examples of structural transitions under acoustic shocked conditions are α-Fe$_2$O$_3$ to Fe$_3$O$_4$,[11] graphite to disordered graphite,[12] B1 to B2 of CdO,[13] anatase to rutile TiO$_2$[14] and NaCl (B1) to Na$_2$Cl$_3$ ($P4/m$).[15] Note that these transitions require several GPa pressures in the cases of static pressure and flyer plate shock compression experiments. Moreover, with the same crystal symmetry, significant morphological transitions have been observed, which are an irregular to rod-shape in L-tyrosine[16] and an irregular to elongated hexagonal-shape in ammonium sulfate.[17] Even though a few reports are available in this domain, a clear picture is yet to be achieved about how acoustic shock waves can trigger such significant changes in the materials that are exposed to a lower number of shocks and shock pressure conditions. To find the major reason for these kinds of structural and morphological changes, many more experiments have to be conducted whereby some possible and logical concepts could be extracted systemically to explain the observed results under acoustic shocked conditions.

Following the previous results, we have chosen powder samples of D-tartaric acid in the present work as it is one of the most important organic compounds in stereochemistry. It is one of the prominent candidates in the pharmaceutical industry as an excipient and buffering agent and possesses potential for technological applications in microelectronics and photonics.[18] From structural chemistry and astrochemistry points of view, it significantly contributes to various aspects such as metal-catalyzed reactions and organocatalysts.[19] Most importantly, in astrochemistry, tartaric acid is a potential molecule to be present in the interstellar medium (ISM), which has already been found in the Murchison meteorite.[20]

From the fundamental and applied research points of view, the title material is a good candidate for investigating its structural stability under acoustic shocked conditions to provide interesting results whereby the shock wave-induced super-heating and melting concepts could be obtained. In the present work, we report the acoustic shock wave-induced melting and dynamic re-crystallization of D-tartaric acid for the first time in the literature, to date, and thereby it is found that it has a stable and ideal crystal structure and morphology under the 100-shocked conditions.

Experimental section

The commercially available fine powder of D-tartaric acid was purchased from Sigma Aldrich Company. The powder was finely ground using a mortar and the obtained powder was utilized as it was for the shock wave recovery experiment. The required shock waves were generated from a tabletop pressure-driven shock tube[21] and the details about the shock tube, such as working methodology, operation and the loading of shock waves are presented in the ESI.† While the atmospheric air was being compressed into the driver section, at the critical pressure, the diaphragm was ruptured such that the shock waves were generated and moved along the driven section. For the shock loading, the sample of dimensions $10 \times 10 \times 1$ mm^3 was rigidly fixed in the sample holder, which was positioned 1 cm apart from the open end of the shock tube. The values of transient pressure and temperature have been calculated by implementing the standard R–H relations as given in the ESI.† For the experimental analysis, Mach number 4.7 shock waves (with a transient pressure and temperature of 16.5 MPa and 3175 K, respectively) were preferred
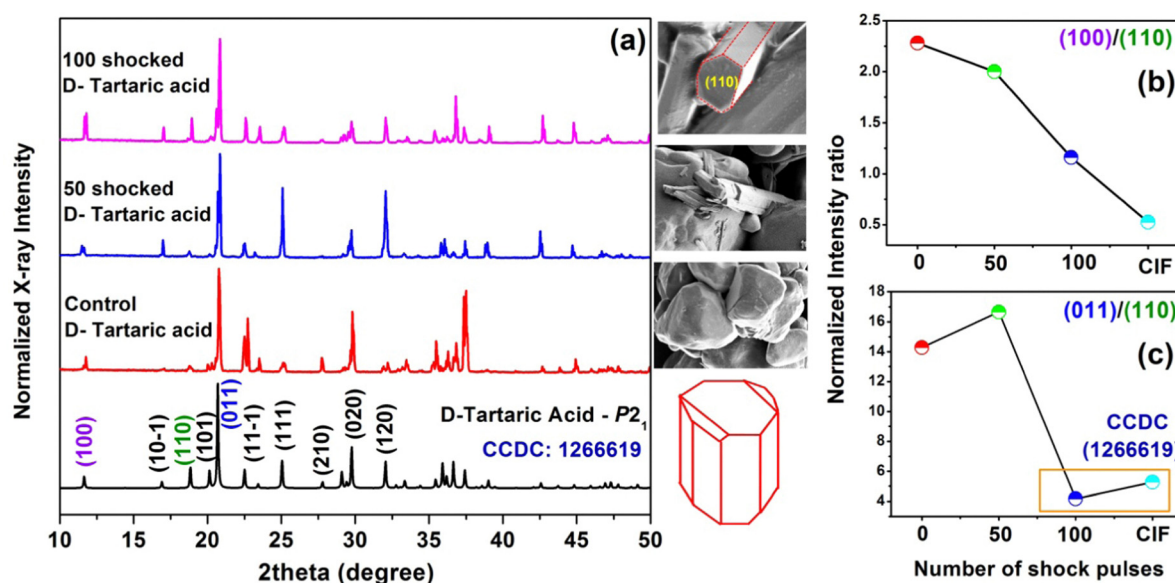
Fig. 1 (a) XRD patterns of the control and shocked D-tartaric acid samples. (b) Intensity ratio of (100)/(110). (c) Intensity ratio of (011)/(110) with respect to the number of shock pulses.

This journal is © the Owner Societies 2025

Phys. Chem. Chem. Phys., 2025, **27**, 308–315 | **309**

such that two different sets of shock pulses with counts of 50 and 100 shocks were exposed on those two samples. Please refer to the ESI† for the complete experimental details of the shock tube, D-tartaric acid, shock wave-loaded conditions and analytical instrument details.

Results and discussion

X-ray diffraction results

Fig. 1a presents the X-ray diffraction patterns of the control and shocked samples of D-tartaric acid. The control sample's XRD line positions are found to be well-matched with the CCDC database: 1266619. Based on the observed XRD lines, it is obvious that the test sample has crystallized in the $P2_1$ crystal symmetry and the lattice dimensions are a = 7.710(3) Å, b = 6.000(3) Å, c = 6.230(3) Å and V = 283.734 Å^3. However, while looking at the intensities and intensity ratio of the diffraction lines of the control sample, it does not match well with the standard XRD pattern (Fig. 1a). The changes in the intensity and intensity ratio of the diffraction lines have significantly affected the external morphology of the crystals leading to morphological transformations without changing the crystal symmetry.[16,17] According to the previous reports,[22,23] the L and D-forms of tartaric acid crystals are crystallized in a rectangular plate-like morphology. However, the control sample does not have a definite rectangular plate-like morphology, whereas it has irregular spherical-shaped particles. The existence of the irregular spherical-shaped morphological pattern is because of the deformations of the major diffraction lines such as (100), (110), (011), *etc.*, in the crystal (Fig. 1a).

Moreover, during the bulk production of such materials, maintaining the typical morphology is much more difficult than maintaining the crystal symmetry, which requires very high precision as well as the optimized synthesizing procedure and similar kinds of results have been observed in L-tyrosine.[16] Under the 50-shocked conditions, the XRD peak positions remain the same; however slight changes have occurred in the peaks' intensity ratios. Specifically, under the 100-shocked conditions, significant modifications have occurred in the intensity ratio which is nearly equal to that of the standard XRD pattern of D-tartaric acid (Fig. 1a). For a better understanding, the normalized intensity ratios of (100)/(110) and (011)/(110) have been calculated and the respective profiles are displayed in Fig. 1b and Fig. 1c. Moreover, under the 100-shocked conditions, the (110) peak intensity has increased significantly, which is a major factor for the plate-like morphology, and the XRD peak intensity and intensity ratio are found to be well-matched with the standard morphology and XRD patterns (Fig. 1c). For a better understanding of the formation of the crystal structure of D-tartaric acid, the Rietveld refinement has been performed for the control and the 100-shocked condition sample and the obtained XRD patterns are portrayed in Fig. 2. The 100 shocked sample has a lower R^2 value compared to the control sample, which clearly demonstrated the formation of a high degree of crystalline nature D-tartaric acid sample and similar kinds of results have been found in L-tyrosine.[16]

Under shocked conditions, considering similar kinds of normalized diffraction planes, changes in the intensity ratio have been found in several molecular crystals and inorganic materials and the observed results are explained in terms of attachment energy as well as preferred orientation growth aspects from the shock wave-induced molten states.[16,17,24,25] For instance, in the case of the potassium dihydrogen phosphate (KDP) and ammonium dihydrogen phosphate (ADP) crystals, two major planes are highly dominant, which actually decide the external surface morphology of the crystals and they are (200) and (101), respectively. Among these planes, the (101) plane has a higher growth rate compared to the (200) plane because of the higher attachment energy. The attachment energies of the (101) and (200) planes for the KDP crystal are found to be 101 and 36 kcal mol^{-1}, respectively. Under acoustic shocked conditions, the (101) plane's intensity is found to have increased and the resultant intensity ratio of (200)/(101) is found
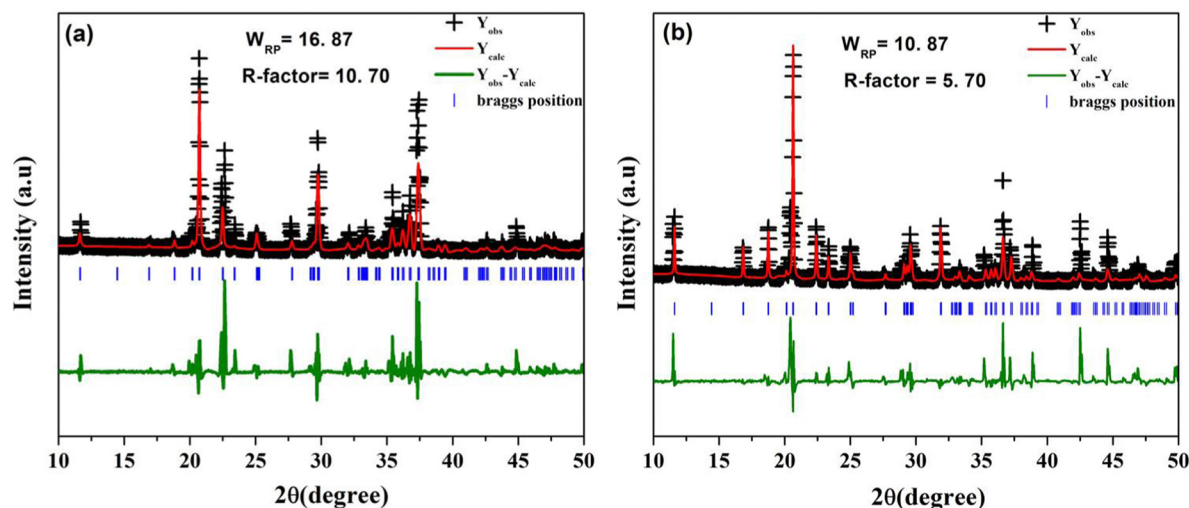
Fig. 2 Rietveld refinement profile of the D-tartaric acid sample: (a) control and (b) 100-shocked sample.

to have reduced with respect to the number of shock pulses[24] and similar kinds of results have been observed in the ADP polycrystalline samples as well.[25] In L-tyrosine, the intensity ratio (130)/(111) of the planes has been found to have significantly reduced under the 200-shocked conditions and the resultant morphological transitions have been observed from irregular to rod shapes.[16]

Raman spectroscopy results

In addition to the XRD results, Raman spectroscopy results also provide phenomenological signatures for the corresponding morphology and the symmetry-related phase transitions of materials and to obtain supporting evidence to the XRD results, the visible Raman spectra have been recorded for the control and shocked samples as presented in Fig. 3a. The control sample's Raman bands and Raman band positions are found to be well-matched with the reported results.[26] However, similar to the XRD results, a significant modification is witnessed in the intensity ratio of the control sample of D-tartaric acid. Among all the Raman lines, a few important Raman lines such as v_{C-O} (1694 and 1700 cm^{-1}), v_{C-H} (2933 and 2967 cm^{-1}) and v_{O-H} (3331 and 3403 cm^{-1}) are considered to justify the existence of lattice deformations in the crystal structure of the control sample. According to the literature, in the v_{C-O} Raman bands, the Raman band of a lower wavenumber should have higher intensity than the Raman band of a higher wavenumber (Fig. 3a). In the v_{C-H} and v_{O-H} Raman bands, the higher wavenumber bands should have higher intensity than the lower wavenumber bands.[26] On the other hand, a complete contrast is witnessed for the intensity ratio profile of the control sample because of the presence of significant lattice deformations. In addition to that, the acidic OH group (v_{O-H}) has the strongest of the hydrogen bonds in the crystal so that they should have relatively sharp bands, whereas, in the control sample, it has very moderate intensity (Fig. 3b). Under shocked conditions, considerable changes have been seen in the intensities and intensity ratios of the Raman bands, especially under the 100-shocked conditions. The zoomed-in versions of the Raman band features of v_{C-H} and v_{O-H} of the control and shocked samples are portrayed in Fig. 3b. Under the 100-shocked conditions, the values of the v_{C-O}, v_{C-H} and v_{O-H} bands' intensity ratio are found to be well-matched with a high degree of crystalline nature of the tartaric acid crystal.[26] In addition, in Fig. 3c, the lattice Raman modes of the control and shocked samples are depicted. For a sample of a high degree of crystalline nature, the optimized morphology should have high intensity internal Raman bands.[26]

However, the control and 50-shocked samples have very moderate intensity lattice Raman bands at 126, 153 and 173 cm^{-1} due to the presence of the deformations. Surprisingly, under the 100-shocked conditions, all the Raman bands have gained higher intensity which authentically represents the formation of nearly the ideal $P2_1$ crystal structure with a near-perfect external morphology.

Microscopic results

From the morphological aspects, two main features of the title sample are highlighted. Firstly, crystals of D-tartaric acid crystallize in a rectangular plate morphology.[22,23] Secondly, the melting point of D-tartaric acid is 444 K.[22] However, in the control sample, the rectangular patterns are not witnessed because of their crystallographic and morphological deformations. The captured morphological features of the control and shocked samples are shown in Fig. 4. Upon the exposure to 50 shocks (Fig. 4b), the
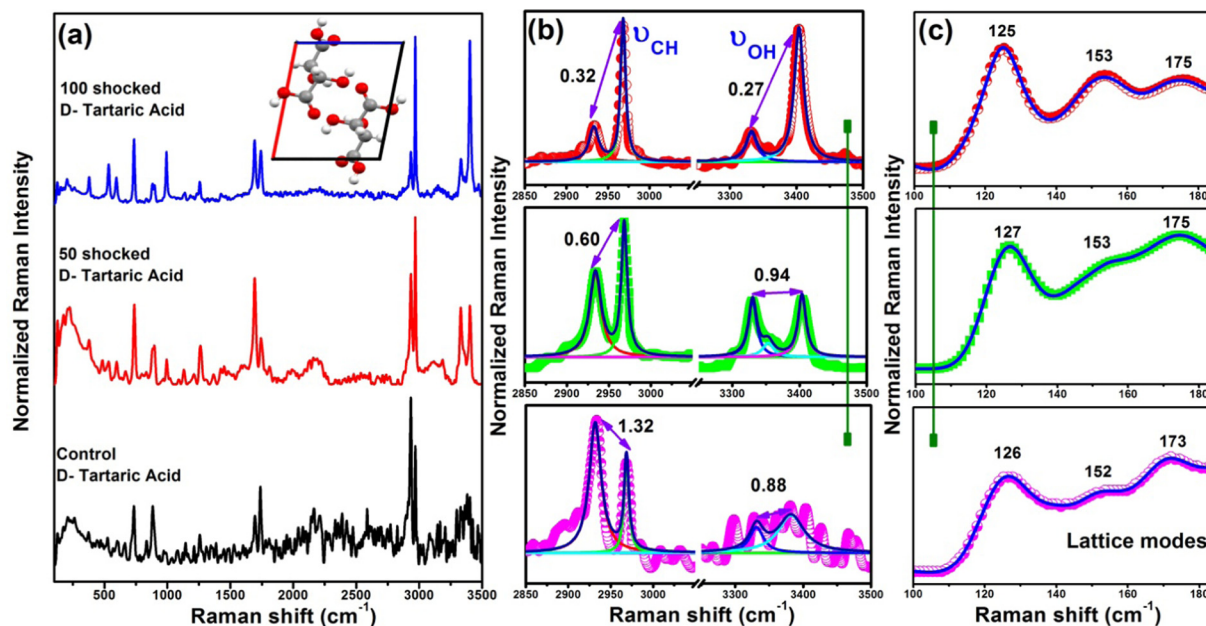
Fig. 3 (a) Raman spectra of the control and shocked D-tartaric acid samples. (b) Zoomed-in versions of the Raman band features 2850–3500 cm^{-1}. (c) Lattice Raman mode features.

This journal is © the Owner Societies 2025

Phys. Chem. Chem. Phys., 2025, **27**, 308–315 | **311**
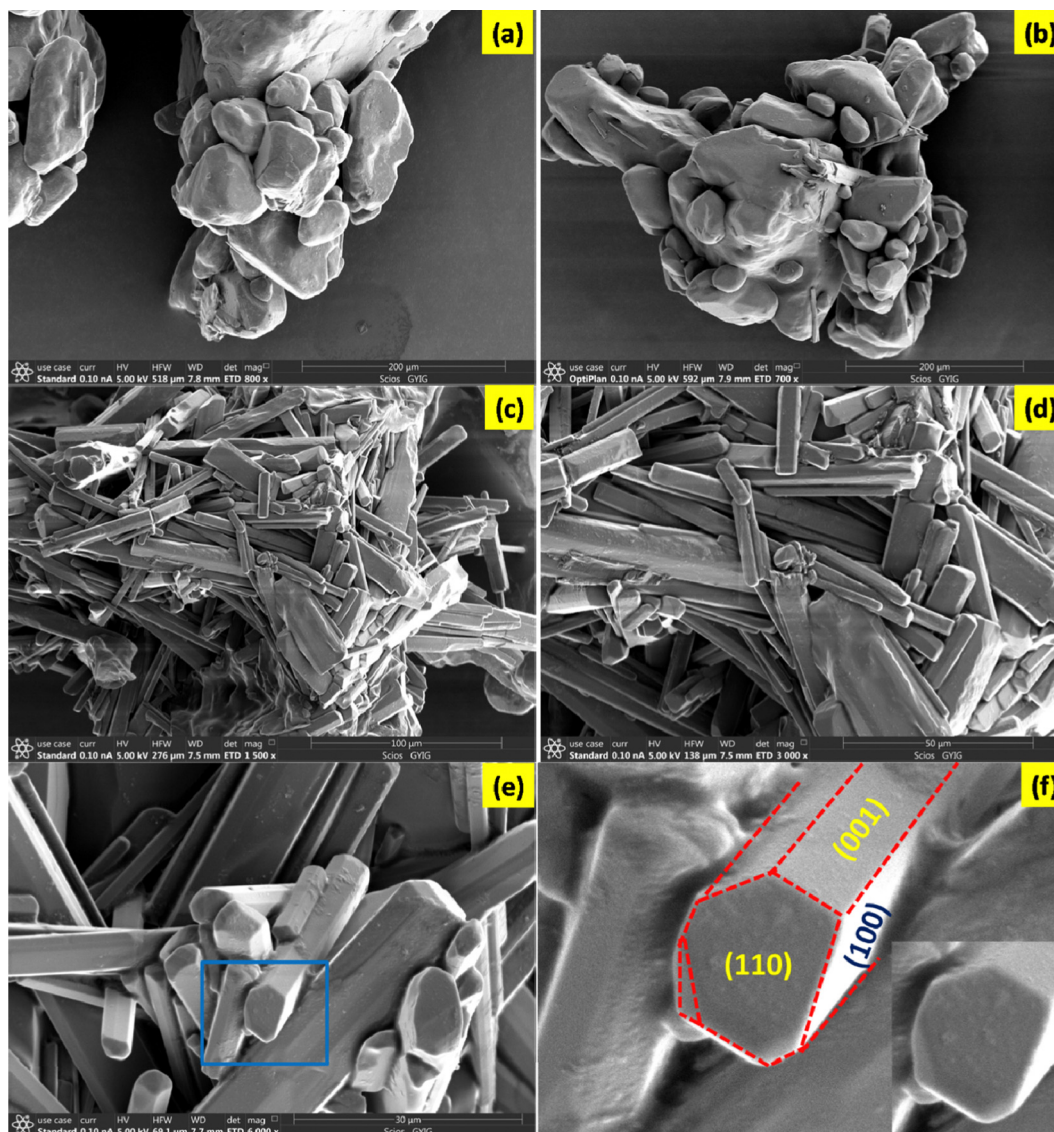
Fig. 4   SEM images of the control and shocked samples: (a) the control, (b) 50-shocked and (c)–(f) 100-shocked.

particles still maintain dominant spherical-shaped morphologies; however, upon the exposure to 100 shocks (Fig. 4c–f), a nearly perfect rectangular plate-like morphology similar to the typical morphology of D-tartaric acid (Fig. 4a) could be seen which is because of the superheating-assisted dynamic recrystallization process induced by the acoustic shock waves.[15–17] The degree of the recrystallization process is directly proportional to the number of shock pulses and the response of materials with respect to the number of shock pulses depends on the initial state of materials wherein the transient pressure and temperature are 16.5 MPa and 3173 K, respectively. The value of transient temperature is 7 fold the equilibrium melting temperature of the title material. Note that, under shocked conditions, materials of lower thermal conductivity experience pre-melting processes because of the shock wave-induced superheating effect, which happens in milliseconds of the transient time scale.

A test sample's pre-melting process can be described as a pre-state of the conventional melting process (molten state), which permits homogenous nucleation during rapid cooling and results in the final phase of the product that is heavily dependent on the interfacial energy between the liquid and solid conditions. Moreover, if the test samples have various defects, such as impurities, interfaces, voids, grain boundaries, and other defects, they significantly reduce the shock heat flow whereby the shock wave heat propagation time scale is slightly prolonged. Due to the combination of the superheating and prolonged time scale of shock wave propagation inside the sample, it receives the required latent heat to initiate melting, which causes the sample to undergo the bulk surface melting transforming into the liquid-like phase easily. Initially, the heat dissipation occurs along the direction of decreasing temperature (the positive temperature gradient is in the direction of the melt) initiating the cooling process after the shock wave propagation. Consequently, a substantial dynamic recrystallization process is set off when the surface transforms into a low-temperature region. During the super-cooling process, the

liquid-like phase is crystallized in the lowest energy state of the test sample with a typical morphology (Fig. 4f).

Note that, due to the fast crystallization process, the initial nuclei may not get enough time to build large-size crystals such that, under the 100-shocked conditions, the size of the crystals is much lower than that of the control sample. The systematic mechanism for the superheating and cooling process based on the thermal conductivity value of the test sample is presented in Fig. 5. From the literature, the value of thermal conductivity of D-tartaric acid could not be found. For L and D-forms of crystal structures, except for their optical activity, the rest of the physical properties such as the melting point, band-gap energy, thermal conductivity, *etc* are highly similar.[18,22] Hence, the thermal conductivity (1.12 W m^{-1} K^{-1}) of L-tartaric acid is considered to explain the super-heating and cooling processes.[27] According to the literature, the thermal conductivity of the materials can be greatly altered by the degree of crystallization, phonon scattering activities, structural defects, impurities, anisotropic nature and existing pressure–temperature of the sample surface.[28–32] If defects and deformations exist in the test sample, the thermal transport process can be greatly affected, leading to many phonon scattering processes in the sample. However, the impact of shock waves can significantly affect such materials with lower thermal transport processing. Note that, under shocked conditions, the applied transient temperature can be easily dissipated

if the test sample possesses higher thermal conductivity and a defect-free lattice. On the other hand, if the test sample has lower thermal conductivity and a defect-free lattice, the applied transient temperature cannot be easily dissipated such that it can sustain for a longer time in the sample, which can contribute to the required latent heat to melt the crystal surface and allow the recrystallization process under the super-cooling conditions. In both aspects, the title material is highly favorable as a test specimen for studying the superheating and cooling processes under acoustic shocked conditions.

Previous findings indicate that even at lower critical shock numbers, materials with lower thermal conductivity experience structural transitions and *vice versa* for materials with higher thermal conductivity.[33] In order to optimize this relation, it is speculated that a material's value of thermal conductivity is inversely proportional to the width of the molten pool. The width of the unstable molten pool caused by shock waves is considered and is divided by several time channels (t_n) at the unit volume. This indicates that the molten pool with a greater width has more time channels ($t_n = 1/k$), and the molten pool with a lower width has fewer time channels (Fig. 5a). Due to the lower thermal transport value and higher molten pool time channels, the supercooling time is slightly higher than the superheating time (Fig. 5b). The molten state is highly unstable and because of its unstable nature, the melt is quickly recrystallized with an
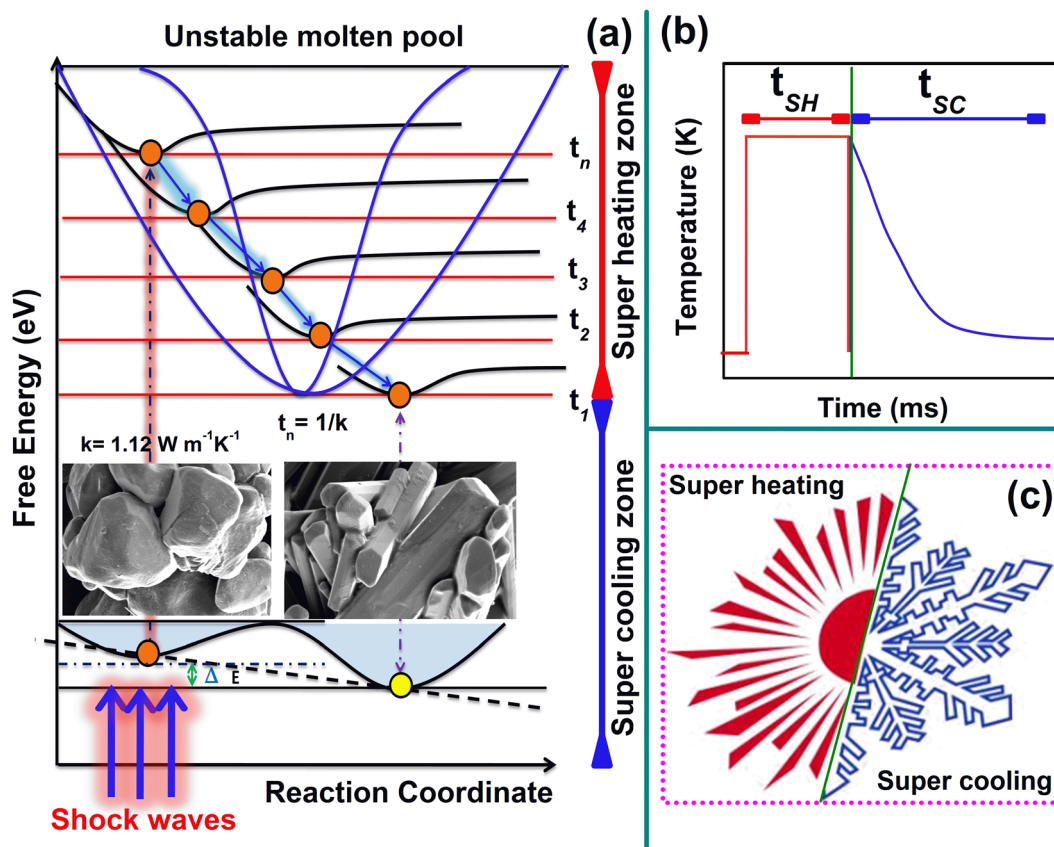
Fig. 5 (a) Thermal conductivity-driven superheating and super-cooling processes of D-tartaric acid under shocked conditions, (b) super-heating and cooling time scale profiles and (c) schematic diagram of super-heating and cooling-assisted crystal growth.

This journal is © the Owner Societies 2025

Phys. Chem. Chem. Phys., 2025, **27**, 308–315 | **313**

associated local-order parameter of the test sample within the millisecond time scale (Fig. 5c).

Conclusion

In the present work, we have systematically demonstrated the acoustic shock wave-induced superheating and cooling processes on the D-tartaric acid powder sample such that the effect of superheating processes has been evaluated by employing diffraction, spectroscopic and microscopic analyses. The 100-shocked sample has a nearly ideal crystal structure of $P2_1$ and a rectangular plate morphology. Note that the typical morphology is highly required along with the crystal symmetry to ensure the potential applications of amino acid and carboxylic acid materials, especially for pharmaceutical applications. In this aspect, the proposed approach is highly suitable to make nearly ideal D-tartaric acid, which can fulfill the requirements of the pharmaceutical industry. Moreover, tabletop shock tube experiments can provide a new direction and option to learn more about superheating of solids, which can bring in a lot of new approaches to understanding this phenomenon better.

Author contributions

L. D. conceived the idea and led the project. S. A. performed the acoustic shock wave measurements. L. D., S. A., S. S. J. D. and R. S. K. contributed to the analysis, interpretation, and discussion of the results. S. A. wrote the manuscript with the help of all the authors. All the authors commented on the final manuscript. L. D. supervised the project.

Data availability

The data that support the findings of this study are available from the corresponding author upon reasonable request.

Conflicts of interest

The authors declare that they have no conflict of interest.

Acknowledgements

References

1 S. N. Luo and T. J. Ahrens, Superheating systematics of crystalline solids, *Appl. Phys. Lett.*, 2003, **82**, 1836.

2 Q. S. Mei and K. Lu, Melting and superheating of crystalline solids: From bulk to Nanocrystals, *Prog. Mater. Sci.*, 2007, **52**, 1175–1262.

3 S. N. Luo and T. J. Ahrens, Shock-induced superheating and melting curves of geophysically important minerals, *Phys. Earth Planet. Inter.*, 2004, **143**, 369–386.

4 S. J. Turneaure, S. M. Sharma and Y. M. Gupta, Nanosecond melting and recrystallization in shock-compressed silicon, *Phys. Rev. Lett.*, 2018, **121**, 135701.

5 H. Iglev, M. Schmeisser, K. Simeonidis, A. Thaller and A. Laubereau, Ultrafast superheating and melting of bulk ice, *Nature*, 2006, **439**, 183–186.

6 B. Rethfeld, K. S. Tinten and D. Linde, Ultrafast thermal melting of laser-excited solids by homogeneous nucleation, *Phys. Rev. B:Condens. Matter Mater. Phys.*, 2002, **65**, 092103.

7 P. Renganathan, S. M. Sharma, S. J. Turneaure and Y. M. Gupta, Real-time (nanoseconds) determination of liquid phase growth during shock-induced melting, *Sci. Adv.*, 2023, **9**, eade5745.

8 S. Aswathappaa, L. Dai, S. S. J. Dhas, S. A. M. B. Dhas, E. Palaniyasan, R. S. Kumar and A. I. Almansour, Synthesis of crystalline graphite from disordered graphite by acoustic shock waves: Hot-spot nucleation approach, *Appl. Surf. Sci.*, 2024, **655**, 159632.

9 V. Jayaram, A. Gupta and K. P. J. Reddy, Investigation of strong shock wave interactions with CeO_2 ceramic, *J. Adv. Ceram*, 2014, **3**, 297–305.

10 A. Sivakumar, S. Soundarya, S. Sahaya Jude Dhas, K. Kamala Bharathi and S. A. Martin Britto Dhas, Shock wave driven solid state phase transformation of Co_3O_4 to CoO nanoparticles, *J. Phys. Chem. C*, 2020, **124**, 10755–10763.

11 A. Sivakumar, A. Rita, S. Sahaya Jude Dhas, K. P. J. Reddy, R. S. Kumar, A. I. Almansour, S. Chakraborty, K. Moovendaran, J. Sridhar and S. A. Martin Britto Dhas, Dynamic shock wave driven simultaneous crystallographic and molecular switching between α-Fe_2O_3 and Fe_3O_4 nanoparticles – a new finding, *Dalton Trans.*, 2022, **51**, 9159–9166.

12 S. Aswathappa, L. Dai, S. A. T. Redfern, S. S. J. Dhas, X. Feng, E. Palaniyasan and R. S. Kumar, Acoustic shock wave-induced sp^2-to-sp^3-type phase transition: a case study of a graphite single crystal, *J. Mater. Chem. C*, 2024, **12**, 14581–14589.

13 S. Aswathappa, L. Dai, S. S. J. Dhas, S. A. M. B. Dhas, S. Laha, R. S. Kumar and A. I. Almansour, Acoustic shock wave-induced solid-state fusion of nanoparticles: a case study of the conversion of one-dimensional rod shape into three-dimensional honeycomb nanostructures of CdO for high performance energy storage materials, *Inorg. Chem.*, 2024, **63**, 576–592.

14 S. Kalaiarasi, A. Sivakumar, S. A. Martin Britto Dhas and M. Jose, Shock wave induced anatase to rutile TiO_2 phase transition using pressure driven shock tube, *Mater. Lett.*, 2018, **219**, 72–75.

15 S. Aswathppa, L. Dai, S. S. J. Dhas, S. A. Martin Britto Dhas, R. S. Kumar and A. A. N. Raj, Acoustic shock wave induced chemical reactions–A case study of NaCl single crystal, *J. Mol. Struct.*, 2024, **1312**, 138490.

16 S. Aswathappa, L. Dai, S. S. J. Dhas, S. A. Martin Britto Dhas, K. K. Bharathi, R. S. Kumar and A. I. Almansour, Experimental demonstration of acoustic shockwave-induced

solid-state morphological transformation from irregular to rod shape: a case study of L-tyrosine, *CrystEngComm*, 2024, **26**, 1199.

17 S. Aswathappa, L. Dai, S. S. J. Dhas, S. A. Martin Britto Dhas, E. Palaniyasan, R. S. Kumar and A. I. Almansour, Experimental evidence of acoustic shock wave-induced dynamic recrystallization: a case study on ammonium sulfate, *Cryst. Growth Des.*, 2024, **24**, 491–498.

18 T. Chen, Q. Zhang, Z. Li, X. Yin and F. Hu, Experimental and theoretical investigations of tartaric acid isomers by terahertz spectroscopy and density functional theory, *Spectrochim. Acta, Part A*, 2018, **205**, 312–319.

19 E. R. Alonso, I. Len, L. Kolesnikov, S. Mata and J. L. Alonso, Unveiling five naked structures of tartaric acid, *Angew. Chem., Int. Ed.*, 2021, **60**, 17410–17414.

20 G. Cooper, N. Kimmich, W. Belisle, J. Sarinana, K. Brabham and L. Garrel, Carbonaceous meteorites as a source of sugar-related organic compounds for the early Earth, *Nature*, 2001, **414**, 879–883.

21 A. Sivakumar, S. Balachandar and S. A. M. B. Dhas, Measurement of ''Shock wave parameters'' in a novel table-top shock tube using microphones, *Hum. Factors Mech. Eng. Def. Saf.*, 2020, **4**, 3.

22 T. Fukami, S. Tahara, C. Yasuda and K. Nakasone, Structural Refinements and Thermal Properties of L(+)-Tartaric, D(−)-Tartaric, and Monohydrate Racemic Tartaric Acid, *Int. J. Chem.*, 2016, **8**, 9–21.

23 K. Moovendaran and S. Natarajan, Unidirectional growth and characterization of L-tartaric acid single crystals, *J. Appl. Cryst.*, 2013, **46**, 993–998.

24 A. Sivakumar, S. Sahaya Jude Dhas, P. Sivaprakash, B. Vigneshwaran, S. Arumugam and S. A. M. B. Dhas, Diffraction and spectroscopic assessment of crystallographic phase stability of potassium dihydrogen phosphate at shocked conditions, *Physica B*, 2022, **627**, 413549.

25 A. Sivakumar, A. Saranraj, S. S. J. Dhas, K. Showrilu and S. A. M. B. Dhas, Phase stability analysis of shocked ammonium dihydrogen phosphate by X-ray and Raman scattering studies, *Z. Kristallogr. – Cryst. Mater.*, 2021, **236**, 1–10.

26 R. Bhattacharjee, Y. S. Jain and H. D. Bist, Laser Raman and infrared spectra of tartaric acid crystals, *J. Raman Spectrosc.*, 1989, **20**, 91–97.

27 T. Jayapalan, S. J. D. Sathiyadhas, J. Michael, B. Settu and M. B. D. S. Amalapushpam, Thermophysical and optical properties of L-tartaric acid crystal, *Cryst. Res. Technol.*, 2018, **53**, 1700267.

28 A. Balandin and K. L. Wang, Significant decrease of the lattice thermal conductivity due to phonon confinement in a free-standing semiconductor quantum well, *Phys. Rev. B: Condens. Matter Mater. Phys.*, 1998, **58**, 1544–1549.

29 O. Delaire, J. Ma, K. Marty, A. F. May, M. A. McGuire, M. H. Du, D. J. Singh, A. Podlesnyak, G. Ehlers, M. D. Lumsden and B. C. Sales, Giant anharmonic phonon scattering in PbTe, *Nat. Mater.*, 2011, **10**, 614–619.

30 E. Borchi, S. De Gennaro, G. Pelosi and A. Rettor, The role of the normal phononphonon scattering in the lattice thermal conductivity and phonondrag in metal at low temperatures, *Phys. Status Solidi B*, 1980, **98**, 667.

31 S. K. Estreicher, T. M. Gibbons, B. Kang and M. B. Bebek, Phonons and defects in semiconductors and nanostructures: Phonon trapping, phonon scattering, and heat flow at heterojunctions, *J. Appl. Phys.*, 2014, **115**, 012012.

32 V. Sivasubramani, S. A. M. B. Dhas, M. S. Pandian and P. Ramasamy, Growth of organic nonlinear optical (NLO) ammonium D, L-Tartrate (AMT) single crystal by conventional and unidirectional method and its characterization, *Mater. Res. Innov.*, 2016, **20**, 67–75.

33 S. Aswathappa, L. Dai, S. J. D. Sathiyadhas, R. S. Kumar and M. V. Reddy, Acoustic shock wave-induced rutile to anatase phase transition of TiO_2 nanoparticles and exploration of their unconventional thermodynamic structural transition path of crystallization behaviors, *Inorg. Chem.*, 2024, **63**, 17043–17055.

This journal is © the Owner Societies 2025

Phys. Chem. Chem. Phys., 2025, **27**, 308–315 | **315**